

LIQUID FRACTION EVOLUTION DURING CASTING OF NI-BASE SUPERALLOYS WITH EMPHASIS ON THE LAST STAGE SOLIDIFICATION

H. B. Dong

Department of Engineering, University of Leicester, University Road, UK

N. D'Souza

Precision Casting Facility, Derby, UK

B. Kantor, P. Hooper

Turbine System Engineering, Bristol, UK

Introduction

Superalloys have been developed over the last 5 decades to meet the increasing demands of improved high temperature creep and fatigue strength required for turbines for both aerospace as well as land-based power generation. INCONEL 713LC (IN713LC) is one of the common superalloys, and it is used extensively for manufacture of blades with equiaxed structure in the low-pressure stage of the turbine for aerospace applications. However, equiaxed solidification is commonly associated with the problem of *hot tearing*, which is an endemic foundry problem.

An extensive program within the Precision Foundry, Rolls-Royce plc, UK to demonstrate equiaxed casting capability of turbine blades corresponding to the low-pressure turbine stage of a developmental aero-engine has identified the dramatic role of minor alloying additions with regards to *hot tearing* propensity within the Ni-base superalloy IN713LC. Hot tearing is a complex defect to predict

since it involves: (a) ability of plastic deformation of the coherent solid dendrite bridges that form during terminal stages of solidification to accommodate deformation, (b) fluid flow in the mushy zone to compensate for deformation and (c) segregation of solute and gaseous elements during final stages of solidification. [1 - 4] It is therefore imperative to understand the evolution of the solid phase during the latter stages of solidification, which is the temperature range where hot tears form. While previous investigations have focused on the role of alloying elements in compositions derived from the alloys IN792, IN718 and IN713LC in dictating the solidification sequence, there have been some drawbacks in the methods employed. [5 - 9] Ordinary quenching experiments, conventional differential thermal analysis (DTA), simple thermodynamic models or pseudo-phase diagram approaches cannot adequately describe the solidification process in multi-component systems. More recently a novel DTA approach has been demonstrated to be a

very potent method in characterising phase transformations and can also be used to calculate the kinetics. [10 -13] This technique takes into account the complete heat flow path within the instrument and also makes use of a sample insertion thermocouple. This approach has been adopted in this analysis. Specifically, the primary aims of this investigation are:

1. To identify the solidification path using an enthalpy-based method that accompanies phase change.
1. To correlate the kinetics of solid phase evolution with extent of micro-segregation during phase transformations.

Table I: Nominal Composition in Weight Percent (wt %) of Alloying Elements in Ni - Base Superalloy IN713LC

Chemistry	C	Al	B	Co	Cr	Fe	Mo	Nb	W	Ti	Zr	Ni
I	0.049	5.84	0.012	0.05	11.8	0.03	4.12	2.1	0.04	0.71	0.108	Bal
II	0.062	6.11	0.008	0.02	11.8	0.04	4.30	2.0	0.03	0.59	0.057	Bal

Experimental method

A Stanton Redcroft 1640 Differential Thermal Analyses unit was used for the experiments incorporating cylindrical samples (diameter 4 mm, height 3mm). All experiments were conducted using a dynamic high purity Ar atmosphere to minimise potential oxidising effects. The unit was calibrated using pure metals with melting points of 1064 °C Au and 1453 °C Ni. Test coupons of required dimension were wire-eroded from as-cast test carrot samples having equiaxed grain structure. The samples were subjected to heating / cooling cycles as follows:

Room temperature → heating (25 K/min) 1000°C → isothermal holding at 1000°C for 10 minutes → heating (5 K/min) 1400°C → isothermal holding at 1400°C for 10 minutes → cooling (5 K/min) 1000°C → isothermal holding at 1000°C for 10 minutes → cooling (25 K/min) room temperature.

Heating and cooling curves were recorded over a series of DTA runs for both alloy chemistries, but only the cooling traces were used for subsequent analyses. A numerical programme *CALCOR* [10-11] was applied to calculate the enthalpy change from the DTA measurements. The programme treats

the complete process of heat flow within the DTA apparatus. This allows the thermal resistances between different parts of the instrument to be calibrated by fitting experimental results for a DTA curve. Details of this method of calibration are available elsewhere. [13-14]

Enthalpy change, specific heat capacity and transition temperatures

Figure 1 shows the measured raw DTA curves: differential signal versus the temperature of sample pan (T_{SP}) during heating and cooling for chemistries I and II. The endothermic peak during heating and exothermic peak during cooling correspond to melting and solidification respectively. In conventional DTA analysis, the measured differential signal is assumed to be proportional to the effective heat capacity difference between the sample and reference. Dong *et al* [10] and Boettinger *et al* [11] pointed out that this is *only true* when no latent heat evolves in the sample and that during melting and solidification of an alloy, and that the measured signal is *smearred* over a range of temperature.

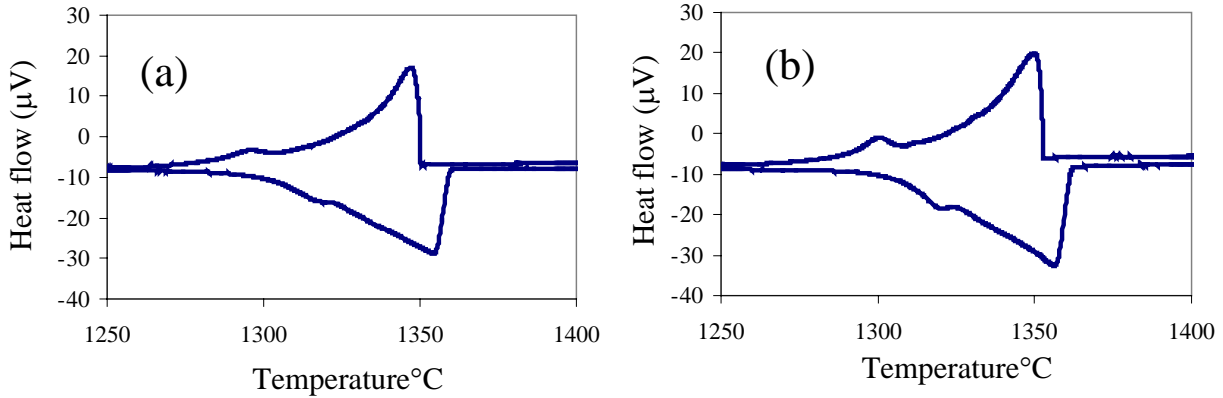


Fig 1. DTA curve showing the raw DTA data (a) chemistry I and (b) chemistry II.

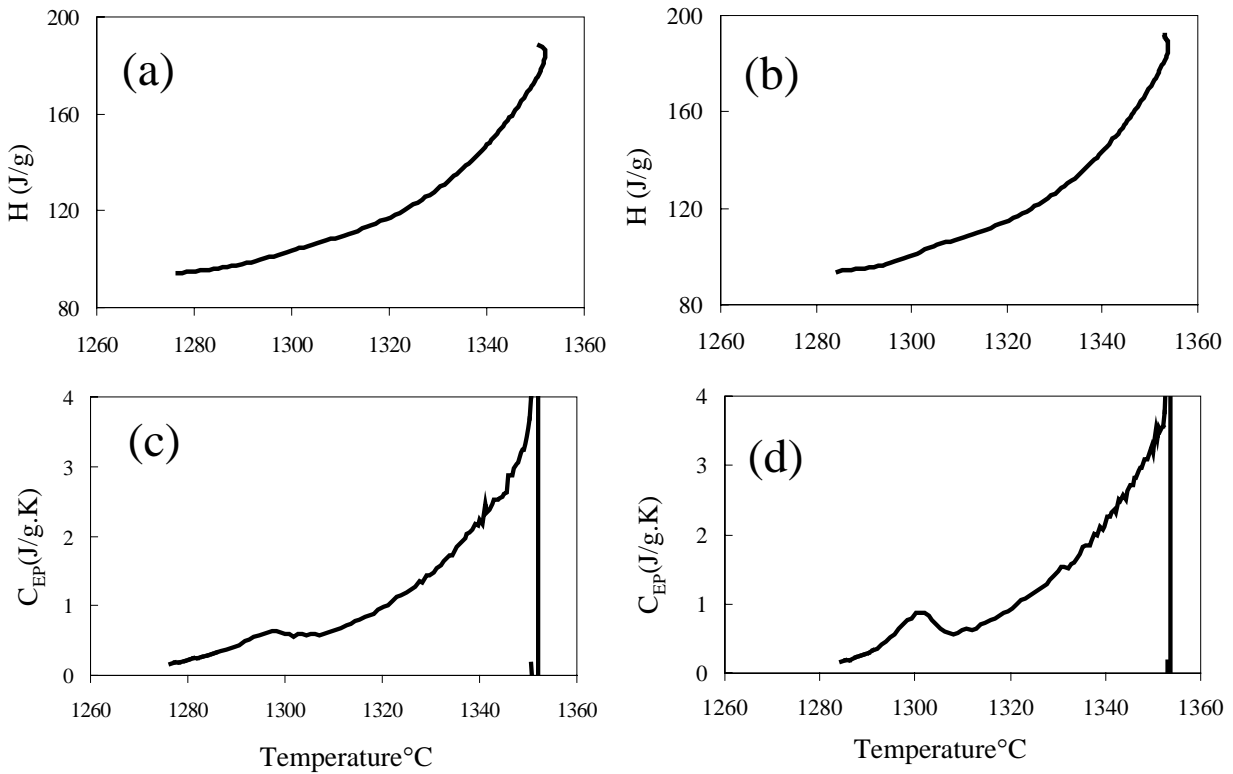


Fig 2. Enthalpy and effective heat capacity curves corresponding to solidification (cooling cycle): (a) and (c) chemistry I; (b) and (d) chemistry II

Therefore in this study the measured raw data was *de-smearred* using the numerical programme *CALCOR* to obtain the sample enthalpy change (H_S) and sample tem

perature (T_S). Figures 2a, b show the calculated H_S versus T_S during the cooling cycle corresponding to chemistries I and II respectively.

The corresponding effective heat capacity

($C_{EP} = \frac{dH}{dT}$) is shown in Figures 2c, d. From the calculated enthalpy curve and heat capacity curve, a *nucleation undercooling* for primary dendrites is 2K for chemistry 1 and 1K for II. However, this undercooling cannot be discerned from the raw data as shown in Figure 1.

Transition temperatures are obtained from the C_{EP} curve corresponding to the cooling cycle i.e. the temperature at which the *effective heat capacity* deviates from baseline. Using this principle:

- i. As shown in Figures 2, solidification commences with a small nucleation in DTA tests, and the liquidus temperatures were deduced as follows: $T_{liquidus} = 1351^{\circ}\text{C}$ (I) and $T_{liquidus} = 1354^{\circ}\text{C}$ (II).
- ii. A secondary reaction is also detected from the C_{EP} curves (Figures 2c,d); however, there exists significant difference between the two chemistries. In the case of chemistry I, a *knee* is observed in the C_{EP} curve, which is followed by a minor peak. The knee is absent in II and the peak being more distinct.

Calculation using the thermodynamic software JMatProTM [12] with non-equilibrium conditions (Scheil-Gulliver module) indicates the precipitation of the MC (M: metal) carbide corresponding to these temperature regimes. The determined temperature ranges for *carbide precipitation* from Figure 2 are summarised as: $T_{Start} = 1306^{\circ}\text{C}$ and $T_{End} = 1296^{\circ}\text{C}$ for alloy (I), while: $T_{Start} = 1310^{\circ}\text{C}$ and $T_{End} = 1302^{\circ}\text{C}$ for alloy (II).

Solidus temperature is always difficult to be determined from DTA measurements since the change in heat capacity at the solidus temperature is gradual. In this study, solidus temperature was determined by inspecting the intersection of the base line and the extrapolated

tangent approximation of the heat capacity curve in an enlarged view. It was found that $T_{solidus}$ obtained in this method was more consistent than that determined using conventional analyses of raw DTA curves. In summary: $T_{solidus} = 1276^{\circ}\text{C}$ (I) and $T_{solidus} = 1286^{\circ}\text{C}$ (II).

It shall be pointed that JMatProTM does not show any difference in enthalpy change, heat capacity and transition temperatures for alloy I and II using either a *Lever* or *Scheil* type analyses.

The obtained enthalpy change, heat capacity and transition temperatures will be used in calculating liquid weight fraction (f_L) evolution in the next section.

Evolution of Weight Fraction Solid (f_S)

The evolution of *weight* fraction solid (f_S) or *weight* fraction liquid ($f_L = 1 - f_S$) has been calculated from the measured enthalpy. We express the enthalpy in the form: $H = (C_P T + L f_L)$, where C_P and L are the specific heat capacity and latent heat respectively. Assumptions: (i) neglect role of micro-segregation, i.e. latent heat is assumed to be constant and (ii) $C_{P\ solid} = C_{P\ liquid}$, i.e. solid and liquid phases have similar specific heat capacities. The fraction liquid can be determined in equation [10]:

$$f_L = \left[\frac{(H - H_{solidus}) - C_P (T - T_{solidus})}{(H_{liquidus} - H_{solidus}) - C_P (T_{liquidus} - T_{solidus})} \right] \quad [1]$$

There may be an inaccuracy in the fraction solid calculation. As it has been demonstrated by Dong *et al* [10] in Al - 4.45 wt % Cu alloys, micro-segregation should be considered in determining the fraction liquid change. However in our calculations, as a first approximation we neglect micro-segregation; the reason being the absence of a comprehensive database capable of treating the enthalpy change as a function of temperature and composition for IN713LC. Similar behaviour is observed in change in f_L as the enthalpy change in Figure 2. However,

significant difference occurs in the rate of fraction solid change at the last stages of solidification ($f_L < 0.1$), which is the regime

where hot tears form. This will be discussed in the next section.

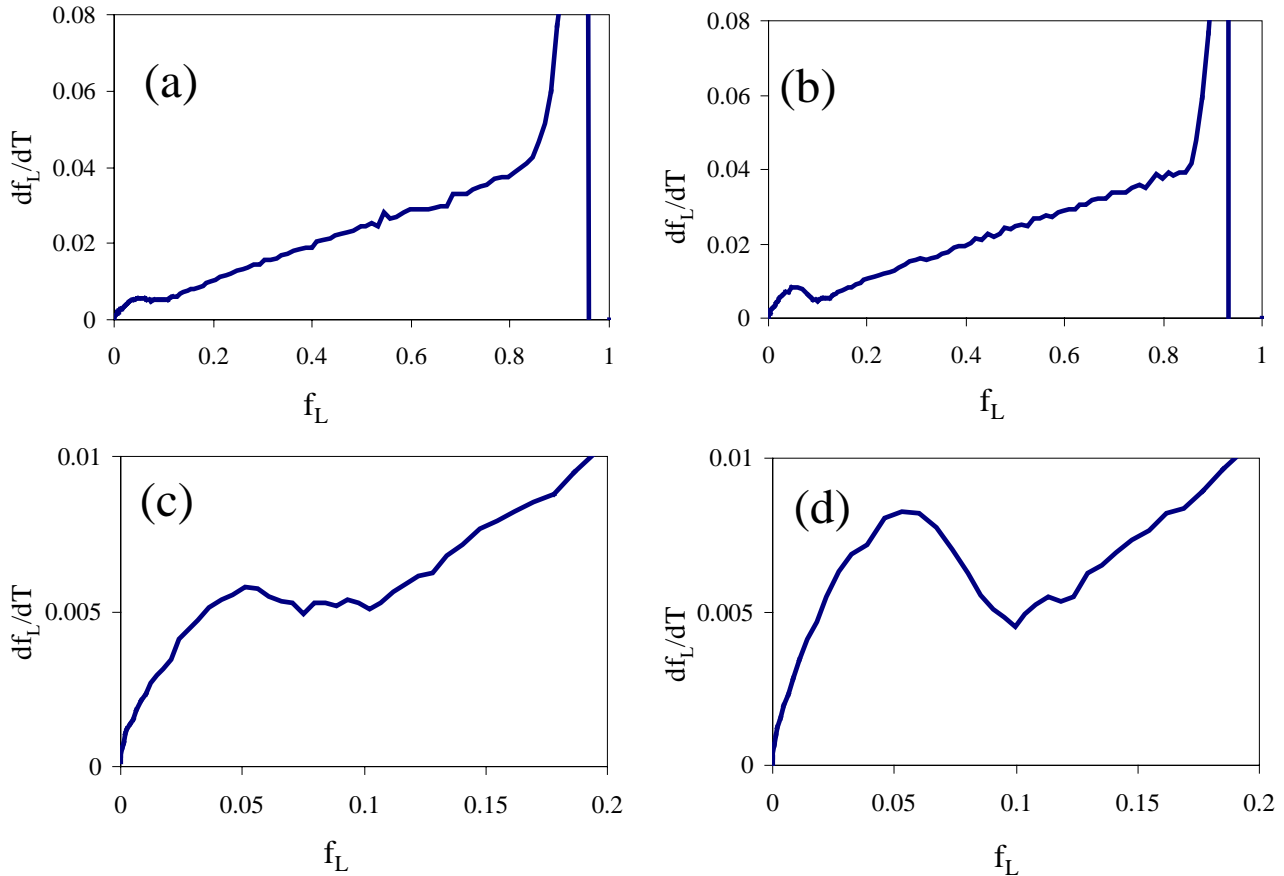


Fig. 3. The rate of fraction liquid change ($\frac{df_L}{dT}$) as a function of fraction liquid (f_L) (a) and (c) chemistry I; (c) and (d) chemistry II.

Rate of Fraction Liquid Change at Last Stages of Solidification

Figure 3a and b shows the rate of fraction liquid change ($\frac{df_L}{dT}$) as a function of fraction liquid (f_L) for alloys I and II (again, constant latent heat is assumed). A detailed analysis corresponding to the last 20% liquid fraction evolution is shown in Figure 3c and d. When $0.1 < f_L < 0.2$, the rate of the fraction liquid changes between the alloy I and alloy II are the same. Significant difference occurs when

$f_L < 0.1$, in alloy 1 the maximum rate is 0.0057 K^{-1} ; while in alloy 2, it is 0.0083 K^{-1} . So the evolution of solid in I accompanying carbide precipitation is *retarded* in relation to II.

Sequence of Solidification

The influence of cooling rate on the temperatures and sequence of phase transformations has been studied by Antonsson and Fredriksson [6] and Bhambri *et al* [7] in IN718 and IN713LC respectively for a wide range; typically $0.10 - 50 \text{ K s}^{-1}$ and shown to have no influence on either the solidification

sequence or degree of micro-segregation. In this investigation, the cooling rate was 0.08 K s^{-1} . The solidification sequence for chemistries I and II has been identified as follows:

(A) $\mathbf{L} \rightarrow \gamma$: Solidification commences with the transition: $\mathbf{L} \rightarrow \gamma$. A small nucleation undercooling ($\Delta T_N \leq 2\text{K}$, section 3.1) has been observed. This is consistent with observations of Bhambri *et al* [7] in IN713LC. They have attributed this effect to the heterogeneous sites presented by un-melted *primary* carbides; these were not observed in our DTA experiments. However, a low interfacial energy between liquid metal and the crucible walls can provide favourable sites for heterogeneous nucleation accounting for the low nucleation undercooling.

(B) $\mathbf{L} \rightarrow \gamma + \mathbf{MC}$: Solidification is progressively accompanied by micro-segregation with a secondary reaction occurring in the range: $0.05 \leq f_L \leq 0.10$ for both alloys. This reaction is of the form: $\mathbf{L} \rightarrow \gamma + \mathbf{MC}$, where $\mathbf{M} = \text{Nb, Zr and Mo}$, with intensity of segregation in descending order. The observed *temperature interval* corresponding to carbide precipitation fits well with that predicted by JMatPro for the two chemistries. Carbides have been detected in both microstructures within the inter-dendritic liquid with primarily *Chinese Script* morphology, as in the high magnification back-scattered electron image (BEI) [Script Mater]. The kinetics of carbide precipitation is retarded in I when compared with II and will be discussed below.

(C) $\mathbf{L} \rightarrow \gamma + \mathbf{MC} + [\gamma - \gamma']$ for II, and $\mathbf{L} \rightarrow \gamma + \mathbf{MC} + [\gamma - \gamma'] + (\mathbf{Zr - Nb rich phase})$ for I: Termination of carbide precipitation corresponds to $f_L = 0.05$, for both chemistries. There is also the appearance of enlarged γ' particles the so-called *primary* γ' , which are deposited in the inter-dendritic liquid during a later stage of solidification. Element analysis using EDS [Script Mater] revealed that the $[\gamma - \gamma']$ eutectic in both alloys is strongly segregated in Zr, Nb and depleted in Cr and pre-

cipitates over a temperature range: $T_{Solidus} \leq T \leq T_{Regime II - End}$. The occurrence of primary γ' can be either be in the vicinity of the fine lamella $[\gamma - \gamma']$ eutectic pool or occur disparately within the inter-dendritic liquid. This constitutes the solidification sequence in chemistry II.

In summary, the formation of the highly segregated phase in chemistry I is a manifestation of the *enhanced micro-segregation* encountered in chemistry I, resulting in retarded solidification kinetics compared with chemistry II, leading to a high *hot tearing* propensity. Further analysis is under way to quantitatively characterise the segregation of Zr and the formation of Zr-Nb rich phase in chemistry I.

Conclusions

The solidification path and a quantitative characterisation of the solidification kinetics during last stage solidification have been presented for two chemistries derived from IN713LC. The enthalpy change and solid fraction evolution were determined using a DTA-based method. The retarded freezing rate of terminal inter-dendritic liquid in the chemistry containing higher Zr arises from increased micro-segregation and results in precipitation of highly segregated $[\text{Zr} - \text{Nb}]$ rich non-equilibrium phase

References

- [1] Rappaz M, Jacot A, Boettinger WJ. Metallurgical and Materials Transactions 2003; 34A: 467.
- [2] Farup I, Drezet J-M, Rappaz M. Acta Materialia 2001; 49: 1261.
- [3] Grasso PD, Drezet J-M, Rappaz M. Journal of Metals (JOM - e) 2002; 1.
- [4] Rappaz M, Drezet J-M, Gremaud M. Metallurgical and Materials Transactions 1999; 30A: 449.
- [5] Sung P. K., Poirier D. R., Felicelli S. D., Poirier E. J., Ahmed A. Journal of Crystal Growth; 2001: 226; 363.
- [6] Antonsson T, Fredriksson H. Metallurgical and Materials Transactions 2005; 36B: 85.

- [7] Bhambri A. K, Kattamis T. Z, Morral J. E. Metallurgical Transactions 1975; 6B: 523.
- [8] Dong HB. PhD Thesis, University of Oxford, Oxford, UK; 2000: 191.
- [9] Dong H. B. and Hunt J. D. J. Therm. Anal. and Cal ; 2001, 64 (1) : 167.
- [10] Dong HB, Shin MRM, Kurum EC, Cama H, and Hunt JD. Metallurgical and Materials Transactions 2003; 34A: 467.
- [11] Boettinger WJ, Kattner UR. Metallurgical and Materials Transactions 2002; 33A: 1779.
- [12] JMatPro™, Ni Module (v. 2.0), Sente Software, Guilford, UK; November 2002.
- [13] D'Souza N., Dong H.B., Ardakani M.G., Shollock B.A., submitted to *Script Mater.*